

Abstract

Secondary organic aerosol (SOA) and oxidized primary organic aerosol (OPOA) were produced in laboratory experiments from the oxidation of fourteen precursors representing atmospherically relevant biogenic and anthropogenic sources. The SOA and OPOA particles were generated via controlled exposure of precursors to OH radicals and/or O₃ in a Potential Aerosol Mass (PAM) flow reactor over timescales equivalent to 1–20 days of atmospheric aging. Aerosol mass spectra of SOA and OPOA were measured with an Aerodyne aerosol mass spectrometer (AMS). The fraction of AMS signal at $m/z = 43$ and $m/z = 44$ (f_{43} , f_{44}), the hydrogen-to-carbon (H/C) ratio, and the oxygen-to-carbon (O/C) ratio of the SOA and OPOA were obtained, which are commonly used to characterize the level of oxidation of oxygenated organic aerosol (OOA). The results show that PAM-generated SOA and OPOA can reproduce and extend the observed $f_{44} - f_{43}$ composition beyond that of ambient OOA as measured by an AMS. Van Krevelen diagrams showing H/C ratio as a function of O/C ratio suggest an oxidation mechanism involving formation of carboxylic acids concurrent with fragmentation of carbon-carbon bonds. Cloud condensation nuclei (CCN) activity of PAM-generated SOA and OPOA was measured as a function of OH exposure and characterized as a function of O/C ratio. CCN activity of the SOA and OPOA, which was characterized in the form of the hygroscopicity parameter κ_{org} , ranged from 0.003 to 0.28 over measured O/C ratios ranging from 0.05 to 1.42. This range of κ_{org} and O/C ratio is significantly wider than has been previously obtained. To first order, the κ_{org} -to-O/C relationship is well represented by a linear function of the form $\kappa_{\text{org}} = (0.17 \pm 0.04) \times \text{O/C} + 0.04$, suggesting that a simple, semi-empirical parameterization of OOA hygroscopicity and oxidation level can be defined for use in chemistry and climate models.

Studies of chemical composition and CCN activity of SOA

A. T. Lambe et al.

Title Page

Abstract

Introduction

Conclusions

References

Tables

Figures

◀

▶

◀

▶

Back

Close

Full Screen / Esc

Printer-friendly Version

Interactive Discussion



1 Introduction

The physical and chemical properties of organic aerosols (OA) are highly complex. Due to atmospheric processes such as dilution, mixing and oxidative aging that result in formation of oxygenated OA (OOA; Zhang et al., 2005), OA properties are highly dynamic, making their characterization challenging. The task is further complicated by limitations in common measurement techniques (often incomplete and indirect) that are typically used to characterize OA in situ. Current knowledge is summarized in several articles (Fuzzi et al., 2006; Kroll and Seinfeld, 2008; Hallquist et al., 2009; Jimenez et al., 2009).

The characterization of OOA in climate models requires simplifying parameterizations of aerosol chemical and physical properties (Kanakidou et al., 2005). Laboratory and field measurements have shown that meaningful simplified representations of OOA chemical composition are possible (Murphy et al., 2006; DeCarlo et al., 2006; Pratt et al., 2009; Hawkins et al., 2010; Mazzoleni et al., 2010). Source apportionment of OOA using Aerodyne aerosol mass spectrometer (AMS) measurements has been widely used over the last several years (e.g. Zhang et al., 2005; Lanz et al., 2007; Hildebrandt et al., 2010). Ng et al. (2010) demonstrated that the measured fraction of AMS organic signals at $m/z = 43$ (f_{43}) and $m/z = 44$ (f_{44}) provide a reasonable representation of the OOA oxidation level. In general, the AMS f_{44} increases and the AMS f_{43} decreases with oxidation level of the OOA. Based on higher mass resolution AMS measurements (Aiken et al., 2010; DeCarlo et al., 2010; He et al., 2010), the increase in f_{44} is interpreted to be due to formation of CO_2^+ ions, while the decrease in f_{43} is due to oxidation of C_3H_7^+ and/or $\text{C}_2\text{H}_3\text{O}^+$ ions. High-resolution AMS measurements have made it possible to obtain more detailed information about OOA chemical composition, leading to other simplifying representations. One such representation, which is not limited to AMS measurements, focuses on the ensemble oxygen-to-carbon (O/C) and hydrogen-to-carbon (H/C) ratios of organic aerosols (Aiken et al., 2008; Wozniak et al., 2008; Heald et al., 2010; Mazzoleni et al., 2010; Kroll et al., 2011).

Studies of chemical composition and CCN activity of SOA

A. T. Lambe et al.

Title Page

Abstract

Introduction

Conclusions

References

Tables

Figures



Back

Close

Full Screen / Esc

Printer-friendly Version

Interactive Discussion



Studies of chemical composition and CCN activity of SOA

A. T. Lambe et al.

Title Page

Abstract

Introduction

Conclusions

References

Tables

Figures

◀

▶

◀

▶

Back

Close

Full Screen / Esc

Printer-friendly Version

Interactive Discussion



Inadequate representation of OOA CCN activity is a potentially large source of uncertainty in climate models (Ghan and Schwartz, 2007; Liu and Wang, 2010). Field experiments have measured OOA with higher CCN activity in air masses that are distant from sources and characterized by increased atmospheric processing (Chang et al., 2010; Wang et al., 2010). Laboratory experiments have also shown that the hygroscopicity of SOA and OPOA increases as a function of oxidant exposure (Huff Hartz et al., 2005; Varutbangkul et al., 2006; Petters et al., 2006; Shilling et al., 2007; Asa-Awuku et al., 2009; Poulain et al., 2010; Engelhart et al., 2011). Therefore, an important objective of ongoing studies is determining simple correlations of relevant chemical and physical properties of OOA using readily measured parameters (Jimenez et al., 2009). A recent study by Massoli et al. (2010) characterized the CCN activity of SOA generated from three precursors over oxidation exposures equivalent to 0.5–10 days of atmospheric aging. Massoli et al. found that CCN activity was positively correlated with the SOA O/C ratio ($O/C = 0.38\text{--}0.98$) and had hygroscopic properties similar to ambient OOA. While these studies have provided a baseline characterization of SOA and OPOA CCN activity, they span a small subset of atmospherically relevant precursors and oxidation timescales.

In the present work, we generate SOA and OPOA from the oxidation of fourteen precursors using a Potential Aerosol Mass (PAM) flow reactor (Kang et al., 2007; Lambe et al., 2011). In addition to SOA generated from the oxidation of well-known volatile organic compound (VOC) precursors, we characterize the properties of SOA generated from oxidation of intermediate volatility organic compounds (IVOC), which have recently been identified as potentially important sources of SOA (Robinson et al., 2007; Chan et al., 2009; Presto et al., 2009; de Gouw et al., 2011). Chemical composition measurements of PAM-generated SOA and OPOA are obtained with the AMS. The f_{44} and f_{43} measurements are correlated with corresponding H/C and O/C ratio measurements to relate unit mass resolution AMS measurements to the more universal H/C and O/C elemental ratios (Ng et al., 2011b). Van Krevelen diagrams are used to provide insight into possible oxidation mechanisms (Krevelen, 1950). The CCN activity

of the SOA and OPOA is characterized using the hygroscopicity parameter κ , and a correlation between κ and O/C ratio is obtained.

2 Experimental methods

2.1 Overview

The SOA and OPOA precursors were oxidized in a PAM flow reactor, which is a horizontal 15 l glass cylindrical chamber 46 cm long \times 22 cm ID. Organic species were transported through the PAM by a carrier gas consisting of 8.5 lpm N_2 and 0.5 lpm O_2 . The average species residence time in the PAM was typically 100 s. Four mercury lamps (BHK Inc.) with peak emission intensity at $\lambda = 254$ nm were mounted in teflon-coated quartz cylindrical sleeves inside the chamber, and were continually purged with N_2 . The size distribution and chemical composition of PAM-generated SOA and OPOA were measured with a combination of a Scanning Mobility Particle Sizer (SMPS, TSI) and an AMS, respectively. The aerosol was size-selected by a DMA (Differential Mobility Analyzer) prior to CCN measurements with a continuous flow CCN counter (CCNC, Droplet Measurement Technologies). A simplified schematic diagram of the experimental setup is shown in Fig. 1. Input lines 1 and 2 provided carrier gases (N_2 , O_2) and OH radical precursors (O_3 , H_2O). Lines 3, 4, and 5 supplied SOA and OPOA precursors that are discussed in Sect. 2.3. Prior to each experiment, the PAM was conditioned with OH radicals until a particle background less than 10 cm^{-3} was attained.

2.2 OH radical generation

OH radicals were produced via the reaction $O_3 + h\nu \rightarrow O_2 + O(^1D)$ followed by the reaction $O(^1D) + H_2O \rightarrow 2OH$. O_3 was generated by irradiating O_2 with a mercury lamp ($\lambda = 185$ nm) outside the PAM. The O_3 concentration was measured using an O_3 monitor (2B Technologies). Oxygen ($O(^1D)$) radicals were produced by UV photolysis

Studies of chemical composition and CCN activity of SOA

A. T. Lambe et al.

Title Page

Abstract

Introduction

Conclusions

References

Tables

Figures

◀

▶

◀

▶

Back

Close

Full Screen / Esc

Printer-friendly Version

Interactive Discussion



of O₃ inside the PAM. The radical O(¹D) then reacted with water vapor (introduced using a heated Nafion membrane humidifier; Perma Pure LLC) to produce OH radicals inside the PAM. The humidifier temperature was set to provide a controlled relative humidity in the range of 30 to 60 %.

The OH exposure, which is the product of the OH concentration and the average residence time in the PAM, was varied by changing the UV light intensity through stepping the voltage applied to the lamps between 0 and 110 V. The OH exposure was obtained indirectly by measuring the decay of SO₂ due to reaction with OH in the PAM. SO₂ calibration measurements were conducted as a function of UV lamp intensity and O₃ concentration (Lambe et al., 2011). Typical OH exposures ranged from $(1.6 \pm 0.8) \times 10^{11}$ to $(2.5 \pm 0.5) \times 10^{12}$ molec cm⁻³ s. Exposures in this range are equivalent to 1–20 days of atmospheric oxidation assuming an average atmospheric OH concentration of 1.5×10^6 molec cm⁻³ (Mao et al., 2009). Both O₃ and OH can oxidize organic species. However, even with O₃ present, OH was the principal oxidant in all experiments except for selected studies with α -pinene and β -pinene, where experiments with O₃ as the oxidizing agent were conducted by turning the lamps off.

2.3 Particle generation

Figure S1 in the Supplement shows molecular structures of SOA and OPOA precursors used in the present work. SOA was generated via gas-phase oxidation of VOCs and IVOCs, and OPOA was generated via heterogenous oxidation of condensed-phase precursors.

The VOC precursors used in this study were *n*-decane (*n*-C₁₀), isoprene, α -pinene, β -pinene, toluene, *m*-xylene, and mesitylene. VOC precursors were prepared in compressed gas cylinders and introduced into the PAM at controlled rates using a mass-flow controller. Depending on the specific study, mixing ratios of the gas-phase precursors entering the PAM ranged from 50 to 330 ppb. The IVOC precursors used in this study were *n*-heptadecane (*n*-C₁₇), diesel fuel, longifolene, and naphthalene. With

Studies of chemical composition and CCN activity of SOA

A. T. Lambe et al.

Title Page

Abstract

Introduction

Conclusions

References

Tables

Figures

◀

▶

◀

▶

Back

Close

Full Screen / Esc

Printer-friendly Version

Interactive Discussion



the exception of naphthalene, IVOCs were introduced into the carrier gas flow using a permeation tube placed in a temperature-controlled oven as described by McKinley (2008). Naphthalene vapor was introduced by flowing N_2 over solid naphthalene placed in a Teflon tube (Chan et al., 2009).

OPOA was generated by heterogenous oxidation of bis(2-ethylhexyl) sebacate (BES) and 10W-30 engine lubricating oil particles. BES and lubricating oil particles were generated via homogenous nucleation in a heated flask. Particles were size-selected with a DMA (TSI 3071A) and were transported through an activated charcoal denuder that removed organic gas-phase species before the particles entered into the PAM. Another set of experiments was conducted with an internally mixed primary aerosol composed of glyoxal and ammonium sulfate. Particles were generated by atomizing an aqueous solution of glyoxal and ammonium sulfate using a constant output atomizer (TSI 3076). While the oxidized glyoxal/sulfate particles are OPOA, we instead refer to this material as SOA to more accurately reflect secondary formation of glyoxal in the atmosphere.

2.4 Particle monitoring and analysis

Particles exiting the PAM chamber passed through an annular denuder filled with Carulite 200 catalyst (Carus Corp.) that selectively removed ozone with a denuding efficiency $>80\%$. Particle number concentrations and size distributions were measured with an SMPS.

The chemical composition of the aerosol was measured with an Aerodyne time-of-flight aerosol mass spectrometer (ToF-AMS) (Drewnick et al., 2005; DeCarlo et al., 2006). Elemental analysis yielding O/C and H/C ratios was performed on high-resolution ToF-AMS (HR-ToF-AMS) measurements. In some experiments this instrument was not available and measurements were performed with a lower resolution compact ToF-AMS (c-ToF-AMS). When using c-ToF-AMS measurements, O/C ratios were obtained from f_{44} measurements that were converted to O/C ratios using specific f_{44} -to-O/C calibration factors for each system. This is an adaptation of the technique

Studies of chemical composition and CCN activity of SOA

A. T. Lambe et al.

Title Page

Abstract

Introduction

Conclusions

References

Tables

Figures

◀

▶

◀

▶

Back

Close

Full Screen / Esc

Printer-friendly Version

Interactive Discussion



described by Aiken et al. (2008), and is discussed in more detail in Sect. 3.2. The CCN activity of particles was measured with a continuous flow CCN counter (CCNC) using a previously described technique (Roberts and Nenes, 2005; Lance et al., 2006). CCN activation curves were generated by systematically varying the CCNC column temperature gradient to obtain controlled water vapor supersaturation between 0.1–1.5% or until 100% activation was reached, whichever occurred first. The CCN hygroscopicity parameter, κ , was calculated using Eq. (1) (Petters and Kreidenweis, 2007):

$$\kappa = \frac{4A^3}{27D_m^3 \ln^2 s_c}; A = \frac{4\sigma_w M_w}{RT \rho_w} \quad (1)$$

Here s_c is the CCNC-measured critical supersaturation, D_m is the dry mobility diameter of the size-selected particles, R is the universal gas constant, T is the sample temperature, and M_w , ρ_w , and σ_w are the molecular weight, density, and surface tension of water ($\sigma_w = 0.072 \text{ J m}^{-2}$).

3 Results and discussion

3.1 PAM-generated SOA/OPOA and its comparison with ambient OOA

As has been stated, the measured fraction of AMS organic signals at $m/z = 43$ (f_{43}) and $= 44$ (f_{44}) provide a reasonable representation of the OOA oxidation level. The f_{43} component provides a measure of less-oxidized, semivolatile OOA while the f_{44} component represents more highly oxidized, low-volatility OOA (Huffman et al., 2009; Jimenez et al., 2009). Results of a thermal denuder experiment, which is described in more detail in the Supplement, are in qualitative accord with this interpretation of the f_{43} and f_{44} components. Briefly, PAM-generated naphthalene and α -pinene SOA were produced at several OH exposures in the PAM and then passed through an Aerodyne thermal denuder (Huffman et al., 2008) set to controlled temperatures ranging from 30

[Title Page](#)[Abstract](#)[Introduction](#)[Conclusions](#)[References](#)[Tables](#)[Figures](#)[⏪](#)[⏩](#)[◀](#)[▶](#)[Back](#)[Close](#)[Full Screen / Esc](#)[Printer-friendly Version](#)[Interactive Discussion](#)

to 250 °C. In each case, the f_{44} -to- f_{43} ratio increased after heating, as shown in Fig. S2 of the Supplement.

Figure 2 shows f_{44} versus f_{43} for SOA and OPOA generated from individual precursors in the PAM. To simplify presentation, the data are displayed in three panels.

Figure 2a shows SOA generated from gas-phase alkanes, and OPOA generated from BES and lubricating oil particles. Figure 2b shows SOA generated from biogenic terpenoid precursors, and Fig. 2c shows SOA produced from aromatic compounds from glyoxal, a known photooxidation product of aromatic compounds (Volkamer et al., 2001; Nishino et al., 2009, 2010). In each figure, SOA/OPOA precursors are designated by symbols shown in the figure inset. The color of the symbols indicates the level of OH exposure in the PAM. Dashed lines indicate the range of f_{44} and f_{43} observed in ambient OA (Ng et al., 2010). In each figure, for comparison, we show f_{44} and f_{43} for an atomized oxalic acid solution (0.36 and 0.00048 respectively) measured in the present work. Oxalic acid is a known oxidation product of aqueous glyoxal (Ervens et al., 2004; Carlton et al., 2007), is often the most abundant dicarboxylic acid in ambient OOA (Sorooshian et al., 2006; Takegawa et al., 2007), and represents the highest oxidation state of atmospheric organics other than CO₂ (Kroll et al., 2011).

The following features are noted in Fig. 2. (1) For all types of PAM-generated SOA, increasing the OH exposure increases f_{44} and decreases f_{43} . However, as will be discussed, f_{43} first increases and then decreases with OH exposure in most cases. (2) For the SOA/OPOA displayed in Fig. 2a and 2b, the measured f_{44} and f_{43} signals span the range observed in ambient OOA as indicated by the dashed lines. For SOA/OPOA generated from precursors shown in Fig. 2c (and for some precursors shown in Fig. 2b), f_{44} and f_{43} extend significantly outside the ambient range as delineated by the dashed-and-dotted boundary lines. (3) With increased OH exposure, f_{44} and f_{43} for all types of PAM-generated SOA/OPOA converge towards the f_{44} and f_{43} of oxalic acid. Table 1, columns 2 and 3 show f_{44} and the corresponding f_{43} measured at the highest OH exposure ($\sim 2 \times 10^{12}$ molec cm⁻³ s) for each type of PAM-generated SOA/OPOA. Likewise, columns 4 and 5 show f_{44} with the corresponding f_{43} obtained at the lowest

Studies of chemical composition and CCN activity of SOA

A. T. Lambe et al.

Title Page

Abstract

Introduction

Conclusions

References

Tables

Figures

◀

▶

◀

▶

Back

Close

Full Screen / Esc

Printer-friendly Version

Interactive Discussion



OH exposure ($\sim 10^{11}$ molec cm $^{-3}$ s). The highest f_{44} and corresponding f_{43} for SOA generated from glyoxal are similar to those obtained for oxalic acid; this result has also been observed by Lee et al. (2011).

Figure 2 and Table 1, column 5 indicate that the f_{43} of PAM-generated SOA/OPOA at low OH exposures varies widely over the range of precursors. This reflects the wide range of precursor structures. The f_{43} spread is particularly wide for SOA generated from aromatic precursors (Fig. 2c). For this class of compounds, f_{43} is low for SOA generated from non-methylated aromatics (naphthalene) and it increases with precursors of increased methylation, reaching a maximum with mesitylene. The range of measured f_{43} decreases with increasing OH exposure, presumably because oxidation converts the lesser-oxidized compounds contributing to f_{43} to products that contribute to f_{44} . Several SOA precursors examined in the present work have been characterized in smog chamber studies (Ng et al., 2010; Chhabra et al., 2011). For a specific precursor, the f_{44} and f_{43} of SOA generated in smog chambers and in the PAM at low OH exposures are generally similar. Because higher OH exposures are possible in the PAM than in smog chambers, the range of attained f_{44} increases significantly.

For PAM-generated SOA obtained from the oxidation of nine of the fourteen precursors studied, f_{43} first increases and then decreases with OH exposure. This change is emphasized in a separate $f_{44} - f_{43}$ graph (Fig. S3 of the Supplement), where data from Fig. 2 are shown to highlight the $f_{44} - f_{43}$ trend for SOA generated from these precursors. High-resolution AMS measurements, which facilitate deconvolution of the total f_{43} signal into separate fractions of organic signal consisting of $C_3H_7^+$ ($f_{C_3H_7^+}$) and $C_2H_3O^+$ ($f_{C_2H_3O^+}$) ion fragments, revealed that the f_{43} curvature arises from the increase and subsequent decrease in $f_{C_2H_3O^+}$ with oxidation. For SOA generated from the oxidation of gas-phase alkanes, both $C_3H_7^+$ and $C_2H_3O^+$ ions contribute appreciable fractions of the total $m/z = 43$ signal at low OH exposures. If $C_2H_3O^+$ contributions to f_{43} are isolated in these systems, the extent of f_{43} curvature increases, as shown in Fig. 3 for SOA generated in the PAM from n -C $_{10}$, n -C $_{17}$, and diesel fuel. The observed trends in f_{43} for these precursors suggest a progression from earlier-generation

Studies of chemical composition and CCN activity of SOA

A. T. Lambe et al.

Title Page

Abstract

Introduction

Conclusions

References

Tables

Figures

◀

▶

◀

▶

Back

Close

Full Screen / Esc

Printer-friendly Version

Interactive Discussion



oxidation products containing higher $f_{C_2H_3O^+}$ towards later-generation oxidation products containing lower $f_{C_2H_3O^+}$. The f_{43} curvature observed in the present work has also been observed in other studies (Kroll et al., 2009; Ng et al., 2010; Chhabra et al., 2011; Lee et al., 2011). However, SOA/OPOA produced from glyoxal, lubricating oil, BES, toluene, and m-xylene did not exhibit the clear f_{43} curvature observed in Fig. S3. For each of these systems, there are plausible explanations for the absence of observable f_{43} curvature. However, we cannot support these explanations without introducing significant speculation to the discussion.

Ambient OOA represents a complex mixture of organics contributed from many precursors. To explore the composition of SOA generated from mixed precursors, we generated SOA from a mixture of ~50 % naphthalene and ~50 % α -pinene at several OH exposures. The f_{44} and f_{43} for this mixture are shown in Fig. 4, together with the f_{44} and f_{43} data (from Fig. 2) of SOA generated separately from naphthalene and α -pinene. The figure shows that mixing two SOA precursors – one generating low- f_{43} SOA and the other generating high- f_{43} SOA – produces SOA with f_{43} approximately averaged between the two components. Specifically, the f_{43} of the naphthalene/ α -pinene SOA mixture ranged from 0.04 to 0.09, which is between the f_{43} of naphthalene SOA and α -pinene SOA at each OH exposure; a similar result was obtained by Lee et al. (2011) from the aqueous OH oxidation of a mixture of glyoxal and pinonic acid. However, f_{44} of the mixture was always lower than f_{44} of naphthalene SOA and α -pinene SOA at a specific OH exposure. This result suggests that a more quantitative understanding of the mixed SOA composition would require knowledge of the yield and volatility of SOA generated from each precursor, which is beyond the scope of this work.

Positive Matrix Factorization (PMF) is a receptor modeling technique used to extract source factors from temporal profiles in field measurements (Paatero and Tapper, 1994). A more detailed comparison of PAM-generated SOA and ambient OA can be obtained using ambient OA factors derived using PMF. With this technique, one can extract mass spectra associated with distinct OA classes: specifically, hydrocarbon-like organic aerosol (HOA), semivolatile OOA (SV-OOA) and low volatility OOA (LV-OOA)

Studies of chemical composition and CCN activity of SOA

A. T. Lambe et al.

Title Page

Abstract

Introduction

Conclusions

References

Tables

Figures

◀

▶

◀

▶

Back

Close

Full Screen / Esc

Printer-friendly Version

Interactive Discussion



(Ulbrich et al., 2009). As was done by Jimenez et al. (2009) and Morgan et al. (2010), we cross-correlated and obtained linear correlation coefficients (r^2) for mass spectra of PAM-generated SOA with mass spectra of composite HOA, SV-OOA, and LV-OOA PMF factors derived from multiple field datasets (Ng et al., 2011a; Ulbrich et al., 2011).

Results are shown in Fig. 5a and 5b for SOA generated in the PAM from α -pinene and n -C₁₇ respectively. SOA generated from α -pinene was well correlated with SV-OOA at low OH exposures ($r^2 = 0.88$ – 0.92) and LV-OOA at high OH exposures ($r^2 = 0.89$ – 0.93). Similar trends were observed for SOA generated from other precursors. As expected, most types of PAM-generated SOA were poorly correlated with HOA, except for SOA generated from alkanes at low OH exposures (e.g. n -C₁₇ as shown in Fig. 5b). These results are consistent with these three PMF factors representing aerosols with increasing residence times in the atmosphere.

3.2 H/C and O/C ratios of PAM-generated SOA and OPOA

An alternate representation of OOA composition uses the Van Krevelen diagram to show changes in the hydrogen-to-carbon (H/C) and oxygen-to-carbon (O/C) ratios as a function of oxidative aging. Because O/C correlates with f_{44} and H/C correlates with f_{43} , (Ng et al., 2011b), the diagram is analogous to the $f_{44} - f_{43}$ representation described earlier. Figure S4a and S4b in the Supplement show O/C ratio as a function of f_{44} and H/C ratio as a function of f_{43} for PAM-generated SOA/OPOA. These figures extend the datasets published by Aiken et al. (2008), Chhabra et al. (2010), and Ng et al. (2011b). Figure S4a shows that with the exception of SOA generated from glyoxal, the O/C – f_{44} relationship is linear for all systems studied and well described by the dashed line in the figure ($O/C = 3.82 \times f_{44} + 0.0794$), which is the best fit to multiple laboratory and field datasets (Aiken et al., 2008). The deviation observed for glyoxal, which was first reported by Chhabra et al. (2010), is due to the high initial oxygen content of glyoxal (O/C \approx 1) despite low f_{44} .

Figure S4b shows that, in general, the relationship between H/C and f_{43} is monotonically increasing but nonlinear. The black dashed line in the figure ($H/C = 1 + 5.16 \times f_{43}$

Studies of chemical composition and CCN activity of SOA

A. T. Lambe et al.

[Title Page](#)[Abstract](#)[Introduction](#)[Conclusions](#)[References](#)[Tables](#)[Figures](#)[◀](#)[▶](#)[◀](#)[▶](#)[Back](#)[Close](#)[Full Screen / Esc](#)[Printer-friendly Version](#)[Interactive Discussion](#)

$-8.85 \times f_{43}^2$) is a quadratic fit to smog chamber and field data (Ng et al., 2011b); grey dashed lines represent $\pm 10\%$ confidence intervals to the quadratic fit as presented by Ng et al. In many cases, PAM-generated SOA/OPOA fall near or within the confidence intervals of the Ng et al. parameterization. Several systems lie well outside the confidence intervals or display different H/C- f_{43} trends, suggesting that in some cases the relationship between H/C ratio and f_{43} is more complicated. For example, SOA generated from glyoxal has significant hydrogen content but does not yield $m/z = 43$ signal; we also note that the H/C ratio of unoxidized glyoxal (H/C ≈ 1.5) is similar to values reported by Chhabra et al. (2010) and may indicate hydration of glyoxal. For OPOA generated from lubricating oil and SOA generated from n -C₁₀, n -C₁₇, and diesel fuel under low oxidation conditions, a significant fraction of the $m/z = 43$ signal consists of C₃H₇⁺ ions. This may not have been the case in systems examined by Ng et al. For OPOA generated from BES, the H/C ratio decreases with increasing f_{43} , a trend which is the opposite of all other types of PAM-generated SOA and OPOA.

Figure 6 contains Van Krevelen diagrams that show H/C versus O/C for SOA/OPOA generated in the PAM from the fourteen precursors shown in Fig. 2 (The reverse of this diagram, i.e. O/C vs. H/C, would provide a closer analogy to the $f_{44} - f_{43}$ relationship displayed in Fig. 2. However, we chose the conventional format that has been used to represent products of coal combustion). To simplify presentation, data are displayed in three panels as was done in Fig. 2. Figure 6a SOA generated from gas-phase alkanes and OPOA generated from lubricating oil and BES particles. Figure 6b shows SOA generated from biogenic terpenoid precursors, and Fig. 6c shows SOA produced from aromatic compounds and from glyoxal. Open symbols represent atomic H/C and O/C ratios of the unoxidized precursors, except for unoxidized lubricating oil, BES, and glyoxal, where open symbols represent measured H/C and O/C ratios. Measured H/C and O/C ratios of oxalic acid are also shown for reference. Dashed lines represent the left- and right-hand sides of the ambient $f_{44} - f_{43}$ triangle converted into Van Krevelen diagram coordinates (Ng et al., 2011b); the grey shaded region indicates the associated uncertainty in converting from f_{44} and f_{43} values to O/C and H/C ratios.

Studies of chemical composition and CCN activity of SOA

A. T. Lambe et al.

Title Page

Abstract

Introduction

Conclusions

References

Tables

Figures

◀

▶

◀

▶

Back

Close

Full Screen / Esc

Printer-friendly Version

Interactive Discussion



Studies of chemical composition and CCN activity of SOA

A. T. Lambe et al.

Title Page

Abstract

Introduction

Conclusions

References

Tables

Figures

◀

▶

◀

▶

Back

Close

Full Screen / Esc

Printer-friendly Version

Interactive Discussion



Consistent with observations discussed in connection with Fig. 2, the following features are noted in Fig. 6. (1) As expected, increasing the OH exposure increases the O/C ratio and, in most cases, decreases the H/C ratio. (2) Measured H/C and O/C ratios of PAM-generated SOA and OPOA span the range observed in ambient OOA as indicated by the dashed lines. (3) For most types of PAM-generated SOA/OPOA, the measured H/C and O/C ratios converge towards the H/C and O/C ratios of oxalic acid.

The rate at which the H/C ratio changes with the O/C ratio in Van Krevelen diagrams can provide information about functional groups that may have formed in the process of oxidation. As discussed in Heald et al. (2010), a slope of zero in Van Krevelen space ($\Delta\text{H/C} = 0$) is consistent with addition of alcohol groups to a carbon backbone. A slope of -2 ($\Delta\text{H/C} = -2 \times \Delta\text{O/C}$) is due to addition of carbonyl groups, and a slope of -1 ($\Delta\text{H/C} = -\Delta\text{O/C}$) is consistent with formation of carboxylic acid groups, or alcohol plus carbonyl groups. As discussed by Ng et al. (2011b), addition of carboxylic acid groups concurrent with C-C bond cleavage can yield slopes between -1 and 0 .

Average (H/C)/(O/C) slopes calculated for PAM-generated SOA and OPOA were obtained from data in Fig. 6 and are shown in Table 2. Consistent with results of Massoli et al. (2010) and Chhabra et al. (2011), most of the measured slopes range from -0.87 to -0.45 , suggesting that oxidative aging in these systems forms primarily carboxylic acid groups (or carbonyl and alcohol groups) and breaks carbon-carbon bonds, leading to fragmentation. Ng et al. (2011b) found (H/C)/(O/C) slopes ≈ -0.5 for ambient OOA, which falls in the midrange of our measurements. The SOA generated from isoprene and gas-phase alkanes have steeper average (H/C)/(O/C) slopes (-0.87 to -0.60) than ambient OOA, particularly at low OH exposures in the PAM, where the H/C ratio decreased faster than at higher OH exposures. As shown in Fig. 6a, the H/C ratios of SOA generated from alkanes and isoprene at low OH exposures range from 1.6 to 2.1 , which is on the high end of H/C ratios typically measured in ambient OOA.

PAM-generated lubricating oil, naphthalene, and glyoxal SOA/OPOA displayed different trends with oxidation. The (H/C)/(O/C) slope of OPOA generated from lubricating oil was -1.7 ± 0.2 . The H/C ratio of SOA generated from naphthalene is lower than

the range of H/C ratios typically measured in ambient OOA. In addition, the H/C ratio of SOA generated from naphthalene did not significantly change with increasing OH exposure, yielding an (H/C)/(O/C) slope of -0.05 ± 0.02 ; similar trends were observed for SOA generated from naphthalene in a smog chamber Chhabra et al. (2011). For SOA generated from glyoxal, the (H/C)/(O/C) slope was -1.2 ± 0.2 , consistent with addition of carboxylic acid groups towards formation of oxalic acid. For several types of PAM-generated SOA, the (H/C)/(O/C) slope changes significantly over the course of oxidation. This evolution suggests that the functional group composition changed as the SOA became more oxidized.

3.3 CCN hygroscopicity parameter (κ_{org}) of PAM-generated SOA and OPOA

Many studies have measured $\kappa_{\text{org}} \approx 0$ for OPOA and $\kappa_{\text{org}} \approx 0.1$ for SOA (e.g. Petters and Kreidenweis, 2007, and references therein). Experimental studies suggest that κ_{org} depends on chemical composition (George et al., 2009; Petters et al., 2009; Chang et al., 2010; Massoli et al., 2010; Engelhart et al., 2011), and the work presented here provides the most extensive evidence that chemical composition influences κ_{org} . Measurements of κ_{org} were made for SOA and OPOA generated from the fourteen precursors listed in Table 1. Figure 7 shows κ_{org} as a function of O/C ratio for PAM-generated SOA/OPOA (except for SOA generated from glyoxal, which is presented and discussed separately later in this section). The results yielded values for the hygroscopicity parameter κ_{org} ranging from 0.003 to 0.28 for O/C ratios that ranged from 0.05 to 1.42. The shaded rectangle in Fig. 7 represents the typical range of ambient O/C ratio and κ_{org} values. The measured κ_{org} for oxalic acid is also shown in Fig. 7, and is in agreement with published values ranging from 0.27 to 0.36 (Petters et al., 2009). Asa-Awuku et al. (2010) and Engelhart et al. (2011) measured $\kappa_{\text{org}} = 0.30$ for the water-soluble fraction of smog-chamber-generated SOA. These results, coupled with the maximum observed $\kappa_{\text{org}} = 0.28$ for PAM-generated SOA, suggest $\kappa_{\text{org}} \approx 0.30$ is an upper-bound value for κ_{org} . The black dashed line in Fig. 7 represents a linear fit applied to the data; grey lines represent $\pm 1\sigma$ confidence bands. The linear fit yields $\kappa_{\text{org}} = (0.17 \pm 0.04) \times \text{O/C} + 0.04$ over the measured range of conditions. To first order,

Studies of chemical composition and CCN activity of SOA

A. T. Lambe et al.

Title Page

Abstract

Introduction

Conclusions

References

Tables

Figures

◀

▶

◀

▶

Back

Close

Full Screen / Esc

Printer-friendly Version

Interactive Discussion



this result suggests that a simple, semi-empirical parameterization of κ_{org} and O/C ratio can be defined for use in chemistry and climate models.

As is evident, for OPOA and SOA with O/C ranging from 0.05 to 0.3, the relationship between κ_{org} and O/C ratio is not encompassed by the linear fit shown in Fig. 7.

This behavior suggests that for these low O/C ratios, κ_{org} may not be fully represented by the O/C ratio. Therefore, the κ_{org} -to-O/C parameterization shown in Fig. 7 is more uncertain for species such as OPOA generated from BES and lubricating oil. However, we note that OOA with such low O/C ratios are typically not observed in ambient measurements (e.g., Ng et al., 2010).

Our results can be compared to previous studies performed over a more limited range of conditions. Chang et al. (2010) measured κ_{org} for ambient OA with O/C ratios ranging from 0.3 to 0.6. They proposed a linear parameterization of the form $\kappa_{\text{org}} = (0.29 \pm 0.05) \times \text{O/C}$ (assuming $\kappa_{\text{org}} = 0$ for $\text{O/C} = 0$). Massoli et al. (2010) measured κ_{org} for PAM-generated SOA with O/C ratios ranging from 0.38 to 0.98. Applying a linear fit to the data presented by Massoli et al. yields $\kappa_{\text{org}} = (0.26 \pm 0.03) \times \text{O/C}$. Jimenez et al. (2009) showed κ_{org} as a function of O/C ratio for multiple smog chamber and field measurements; applying a linear fit to the data yields $\kappa_{\text{org}} = (0.37 \pm 0.09) \times \text{O/C} - 0.06$. We note that κ_{org} values presented in Jimenez et al. are derived from hygroscopic growth factor measurements, which tend to yield lower κ_{org} values than corresponding CCN measurements (Massoli et al., 2010). In several studies, κ_{org} was measured for SOA and OPOA generated in flow tubes and smog chambers (Huff Hartz et al., 2005; King et al., 2007; Prenni et al., 2007; George et al., 2009; Engelhart et al., 2011). In these studies, κ_{org} values fall in the range observed in the present work. However, the range of O/C ratios was not adequate for the formulation of a quantitative relationship with respect to κ_{org} .

In most cases, atmospheric aerosol is a mixture of organic and inorganic material, with inorganics being significantly more hygroscopic than organics. In this regard, it is important to evaluate the κ_{org} – O/C parameterization shown in Fig. 7 in the context of inorganics mixed with OOA. Figure 8 shows the calculated fractional contribution

Studies of chemical composition and CCN activity of SOA

A. T. Lambe et al.

Title Page

Abstract

Introduction

Conclusions

References

Tables

Figures

◀

▶

◀

▶

Back

Close

Full Screen / Esc

Printer-friendly Version

Interactive Discussion



Studies of chemical composition and CCN activity of SOA

A. T. Lambe et al.

Title Page

Abstract

Introduction

Conclusions

References

Tables

Figures

◀

▶

◀

▶

Back

Close

Full Screen / Esc

Printer-friendly Version

Interactive Discussion



of OOA to the κ -values of a mixture of ammonium sulfate and OOA ($\kappa_{\text{sulfate}} = 0.6$) as a function of the volume fraction of organics, assuming linear volume-weighted OOA and sulfate contributions to κ (King et al., 2007, 2010; Dusek et al., 2010; Prisle et al., 2010). Two lines are shown for theoretical mixtures containing sulfate and OOA with O/C ratios of 0.3 and 1.0, respectively (the most common range of O/C in ambient OOA). Data for a mixture of ammonium sulfate and glyoxal are also shown (diamond symbols), which were derived from measured mixture κ -values. For these data, O/C ratio increased from 1.06 to 1.50 as a function of OH exposure. The organic volume fraction of SOA generated from glyoxal also decreased from 0.53 to 0.04 as a function of oxidation.

The κ_{org} – O/C parameterization described previously was used to calculate κ_{org} for the two theoretical OOA/sulfate mixtures and for SOA generated from glyoxal. As is evident from Fig. 8, for an O/C ratio of 0.3, OOA contributions to κ are significant (>20%) when the organic fraction is greater than 0.6. For an O/C ratio of 1.0, OOA contributions to κ are significant when the organic fraction is greater than 0.4. Prenni et al. (2007) showed that SOA contributions to κ -values for mixed SOA-sulfate particles were significant when the organic fraction was greater than 0.6; however the O/C ratio in those experiments was not available. Calculations in Fig. 8 therefore indicate the approximate range of O/C ratios and organic volume fractions where explicit treatment of κ_{org} as a function of O/C ratio is necessary.

4 Summary

Our results show that PAM-generated SOA and OPOA can reproduce and extend beyond the range of $f_{44} - f_{43}$ composition observed in smog chamber and ambient studies. Several types of PAM-generated SOA displayed f_{43} curvature as a function of OH exposure, with f_{43} initially increasing prior to decreasing with continued oxidation. This trend suggests a progression from earlier-generation oxidation products containing higher f_{43} (specifically, $\text{C}_2\text{H}_3\text{O}^+$ ions) towards later-generation oxidation products containing lower f_{43} .

Studies of chemical composition and CCN activity of SOA

A. T. Lambe et al.

Title Page

Abstract

Introduction

Conclusions

References

Tables

Figures

◀

▶

◀

▶

Back

Close

Full Screen / Esc

Printer-friendly Version

Interactive Discussion

Mixing PAM-generated SOA containing low and high f_{43} produced SOA with intermediate f_{43} . Because ambient OOA contains organics from multiple precursors, the corresponding $f_{44} - f_{43}$ composition may provide information about OOA contributions from specific precursors. Measurements from the present work suggest that OOA lying towards the left edge of the ambient $f_{44} - f_{43}$ triangle may be influenced by non-methylated aromatic precursors and/or glyoxal. Similarly, OOA that lies towards the right edge of the triangle may be influenced by methylated aromatic, biogenic, and/or alkane precursors. Inside the ambient $f_{44} - f_{43}$ triangle, OOA may be influenced by a mixture of precursors that individually form OOA lying towards both the left and right edges of the triangle.

Van Krevelen diagrams of PAM-generated SOA/OPOA showed that the H/C ratio usually decreased and the O/C ratio increased with oxidation. The corresponding (H/C)/(O/C) slopes suggest an oxidation mechanism involving formation of carboxylic acids concurrent with fragmentation of carbon-carbon bonds, which is consistent with ambient OOA measurements. The H/C and O/C ratios of SOA/OPOA generated from naphthalene, glyoxal, and lubricating oil evolved at rates that were different from the other systems examined, possibly indicating different oxidation mechanisms. As with the $f_{44} - f_{43}$ triangle, the position of OOA in Van Krevelen diagrams may provide information about contributions from specific precursors.

The work presented here provides the most extensive evidence that κ_{org} depends on chemical composition, as has been suggested by previous studies. The hygroscopicity parameter κ_{org} can be represented by a linear function of the O/C ratio as $\kappa_{\text{org}} = (0.17 \pm 0.04) \times \text{O/C} + 0.04$. Parameterizations in this form may be implemented in climate models because the O/C ratio of organic aerosols is easily measured, whereas other parameters relevant to κ -Köhler theory, such as average molar volume, are difficult to obtain. Therefore, the O/C ratio of OOA may represent a convenient surrogate for other underlying parameters that govern the Köhler behavior of the OOA.

Supplementary material related to this article is available online at:
[http://www.atmos-chem-phys-discuss.net/11/13617/2011/
acpd-11-13617-2011-supplement.pdf](http://www.atmos-chem-phys-discuss.net/11/13617/2011/acpd-11-13617-2011-supplement.pdf).

Acknowledgements. We thank Tiffany Samuelson, Kenneth Christian, and Diana van Duin (Pennsylvania State University) for preparing compressed VOC canisters. We thank Jon Franklin and Scott Herndon (ARI) for building permeation tube ovens used in the present work, and are grateful to Nga Lee Ng and Manjula Canagaratna (ARI) for helpful discussions. This research was supported by the Office of Science (BER), Department of Energy (Atmospheric Science Program) grant No. DE-FG02-05ER63995 and the Atmospheric Chemistry Program of the National Science Foundation grants No. ATM-0525355 and ATM-0854916 to Boston College and Aerodyne Research, Inc.

References

- Aiken, A., DeCarlo, P., Kroll, J., Worsnop, D., Huffman, J., Docherty, K., Ulbrich, I., Mohr, C., Kimmel, J., and Sueper, D.: O/C and OM/OC ratios of primary, secondary, and ambient organic aerosols with high-resolution time-of-flight aerosol mass spectrometry, *Environ. Sci. Technol.*, 42, 4478–4485, 2008. 13619, 13624, 13628
- Aiken, A. C., de Foy, B., Wiedinmyer, C., DeCarlo, P. F., Ulbrich, I. M., Wehrli, M. N., Szidat, S., Prevot, A. S. H., Noda, J., Wacker, L., Volkamer, R., Fortner, E., Wang, J., Laskin, A., Shutthanandan, V., Zheng, J., Zhang, R., Paredes-Miranda, G., Arnott, W. P., Molina, L. T., Sosa, G., Querol, X., and Jimenez, J. L.: Mexico city aerosol analysis during MILAGRO using high resolution aerosol mass spectrometry at the urban supersite (T0) – Part 2: Analysis of the biomass burning contribution and the non-fossil carbon fraction, *Atmos. Chem. Phys.*, 10, 5315–5341, doi:10.5194/acp-10-5315-2010, 2010. 13619
- Asa-Awuku, A., Engelhart, G. J., Lee, B. H., Pandis, S. N., and Nenes, A.: Relating CCN activity, volatility, and droplet growth kinetics of β -caryophyllene secondary organic aerosol, *Atmos. Chem. Phys.*, 9, 795–812, doi:10.5194/acp-9-795-2009, 2009. 13620
- Asa-Awuku, A., Nenes, A., Gao, S., Flagan, R. C., and Seinfeld, J. H.: Water-soluble SOA from Alkene ozonolysis: composition and droplet activation kinetics inferences from analysis of

Studies of chemical composition and CCN activity of SOA

A. T. Lambe et al.

Title Page

Abstract

Introduction

Conclusions

References

Tables

Figures

◀

▶

◀

▶

Back

Close

Full Screen / Esc

Printer-friendly Version

Interactive Discussion



Studies of chemical composition and CCN activity of SOA

A. T. Lambe et al.

Title Page

Abstract

Introduction

Conclusions

References

Tables

Figures

◀

▶

◀

▶

Back

Close

Full Screen / Esc

Printer-friendly Version

Interactive Discussion



CCN activity, *Atmos. Chem. Phys.*, 10, 1585–1597, doi:10.5194/acp-10-1585-2010, 2010. 13631

Carlton, A., Turpin, B., Altieri, K., Seitzinger, S., Reff, A., Lim, H., and Ervens, B.: Atmospheric oxalic acid and SOA production from glyoxal: results of aqueous photooxidation experiments, *Atmos. Environ.*, 41, 7588–7602, 2007. 13625

Chan, A. W. H., Kautzman, K. E., Chhabra, P. S., Surratt, J. D., Chan, M. N., Crouse, J. D., Kürten, A., Wennberg, P. O., Flagan, R. C., and Seinfeld, J. H.: Secondary organic aerosol formation from photooxidation of naphthalene and alkyl-naphthalenes: implications for oxidation of intermediate volatility organic compounds (IVOCs), *Atmos. Chem. Phys.*, 9, 3049–3060, doi:10.5194/acp-9-3049-2009, 2009. 13620, 13623

Chang, R. Y.-W., Slowik, J. G., Shantz, N. C., Vlasenko, A., Liggio, J., Sjostedt, S. J., Leaitch, W. R., and Abbatt, J. P. D.: The hygroscopicity parameter (κ) of ambient organic aerosol at a field site subject to biogenic and anthropogenic influences: relationship to degree of aerosol oxidation, *Atmos. Chem. Phys.*, 10, 5047–5064, doi:10.5194/acp-10-5047-2010, 2010. 13620, 13631, 13632

Chhabra, P. S., Flagan, R. C., and Seinfeld, J. H.: Elemental analysis of chamber organic aerosol using an aerodyne high-resolution aerosol mass spectrometer, *Atmos. Chem. Phys.*, 10, 4111–4131, doi:10.5194/acp-10-4111-2010, 2010. 13628, 13629

Chhabra, P. S., Ng, N. L., Canagaratna, M. R., Corrigan, A. L., Russell, L. M., Worsnop, D. R., Flagan, R. C., and Seinfeld, J. H.: Elemental composition and oxidation of chamber organic aerosol, *Atmos. Chem. Phys. Discuss.*, 11, 10305–10342, doi:10.5194/acpd-11-10305-2011, 2011. 13626, 13627, 13630, 13631

de Gouw, J. A., Middlebrook, A. M., Warneke, C., Ahmadov, R., Atlas, E. L., Bahreini, R., Blake, D. R., Brock, C. A., Brioude, J., Fahey, D. W., Fehsenfeld, F. C., Holloway, J. S., Henaff, M. L., Lueb, R. A., McKeen, S. A., Meagher, J. F., Murphy, D. M., Paris, C., Parrish, D. D., Perring, A. E., Pollack, I. B., Ravishankara, A. R., Robinson, A. L., Ryerson, T. B., Schwarz, J. P., Spackman, J. R., Srinivasan, A., and Watts, L. A.: Organic aerosol formation downwind from the Deepwater Horizon oil spill, *Science*, 331, 1295–1299, doi:10.1126/science.1200320, 2011. 13620

DeCarlo, P. F., Kimmel, J. R., Trimborn, A., Northway, M. J., Jayne, J. T., Aiken, A. C., Gonin, M., Fuhrer, K., Horvath, T., Docherty, K. S., Worsnop, D. R., and Jimenez, J. L.: Field-deployable, high-resolution, time-of-flight aerosol mass spectrometer, *Anal. Chem.*, 78, 8281–8289, doi:10.1021/ac061249n, 2006. 13623

Studies of chemical composition and CCN activity of SOA

A. T. Lambe et al.

Title Page

Abstract

Introduction

Conclusions

References

Tables

Figures

◀

▶

◀

▶

Back

Close

Full Screen / Esc

Printer-friendly Version

Interactive Discussion



- DeCarlo, P. F., Ulbrich, I. M., Crounse, J., de Foy, B., Dunlea, E. J., Aiken, A. C., Knapp, D., Weinheimer, A. J., Campos, T., Wennberg, P. O., and Jimenez, J. L.: Investigation of the sources and processing of organic aerosol over the Central Mexican Plateau from aircraft measurements during MILAGRO, *Atmos. Chem. Phys.*, 10, 5257–5280, doi:10.5194/acp-10-5257-2010, 2010. 13619
- 5 Drewnick, F., Hings, S., DeCarlo, P., Jayne, J., Gonin, M., Fuhrer, K., Weimer, S., Jimenez, J., Demerjian, K., Borrmann, S., and Worsnop, D.: A new time-of-flight aerosol mass spectrometer (TOF-AMS) – instrument description and first field deployment, *Aerosol Sci. Technol.*, 39, 637–658, doi:10.1080/02786820500182040, 2005. 13623
- 10 Dusek, U., Frank, G. P., Curtius, J., Drewnick, F., Schneider, J., Kürten, A., Rose, D., Andreae, M. O., Borrmann, S., and Pöschl, U.: Enhanced organic mass fraction and decreased hygroscopicity of cloud condensation nuclei (CCN) during new particle formation events, *Geophys. Res. Lett.*, 37, L03804, doi:10.1029/2009GL040930, 2010. 13633
- Engelhart, G. J., Moore, R. H., Nenes, A., and Pandis, S. N.: Cloud condensation nuclei activity of isoprene secondary organic aerosol, *J. Geophys. Res.*, 116, D02207, doi:10.1029/2010JD014706, 2011. 13620, 13631, 13632
- 15 Ervens, B., Feingold, G., Frost, G. J., and Kreidenweis, S. M.: A modeling study of aqueous production of dicarboxylic acids: 1. Chemical pathways and speciated organic mass production, *J. Geophys. Res.*, 109, D15205, doi:10.1029/2003JD004387, 2004. 13625
- 20 Fuzzi, S., Andreae, M. O., Huebert, B. J., Kulmala, M., Bond, T. C., Boy, M., Doherty, S. J., Guenther, A., Kanakidou, M., Kawamura, K., Kerminen, V.-M., Lohmann, U., Russell, L. M., and Pöschl, U.: Critical assessment of the current state of scientific knowledge, terminology, and research needs concerning the role of organic aerosols in the atmosphere, climate, and global change, *Atmos. Chem. Phys.*, 6, 2017–2038, doi:10.5194/acp-6-2017-2006, 2006. 13619
- 25 George, I. J., Chang, R. Y. W., Danov, V., Vlasenko, A., and Abbatt, J. P. D.: Modification of cloud condensation nucleus activity of organic aerosols by hydroxyl radical heterogeneous oxidation, *Atmos. Environ.*, 43, 5038–5045, doi:10.1016/j.atmosenv.2009.06.043, 2009. 13631, 13632
- 30 Ghan, S. and Schwartz, S.: Aerosol properties and processes, *B. Am. Meteor. Soc.*, 88, 1059–1083, 2007. 13620
- Hallquist, M., Wenger, J. C., Baltensperger, U., Rudich, Y., Simpson, D., Claeys, M., Dommen, J., Donahue, N. M., George, C., Goldstein, A. H., Hamilton, J. F., Herrmann, H., Hoffmann,

Studies of chemical composition and CCN activity of SOA

A. T. Lambe et al.

Title Page

Abstract

Introduction

Conclusions

References

Tables

Figures

◀

▶

◀

▶

Back

Close

Full Screen / Esc

Printer-friendly Version

Interactive Discussion

T., Iinuma, Y., Jang, M., Jenkin, M. E., Jimenez, J. L., Kiendler-Scharr, A., Maenhaut, W., McFiggans, G., Mentel, Th. F., Monod, A., Prévôt, A. S. H., Seinfeld, J. H., Surratt, J. D., Szmigielski, R., and Wildt, J.: The formation, properties and impact of secondary organic aerosol: current and emerging issues, *Atmos. Chem. Phys.*, 9, 5155–5236, doi:10.5194/acp-9-5155-2009, 2009. 13619

He, L.-Y., Lin, Y., Huang, X.-F., Guo, S., Xue, L., Su, Q., Hu, M., Luan, S.-J., and Zhang, Y.-H.: Characterization of high-resolution aerosol mass spectra of primary organic aerosol emissions from Chinese cooking and biomass burning, *Atmos. Chem. Phys.*, 10, 11535–11543, doi:10.5194/acp-10-11535-2010, 2010. 13619

Heald, C. L., Kroll, J. H., Jimenez, J. L., Docherty, K. S., Decarlo, P. F., Aiken, A. C., Chen, Q., Martin, S. T., Farmer, D. K., and Artaxo, P.: A simplified description of the evolution of organic aerosol composition in the atmosphere, *Geophys. Res. Lett.*, 37, L08803, doi:10.1029/2010GL042737, 2010. 13619, 13630

Hildebrandt, L., Engelhart, G. J., Mohr, C., Kostenidou, E., Lanz, V. A., Bougiatioti, A., DeCarlo, P. F., Prevot, A. S. H., Baltensperger, U., Mihalopoulos, N., Donahue, N. M., and Pandis, S. N.: Aged organic aerosol in the Eastern Mediterranean: the Finokalia Aerosol Measurement Experiment 2008, *Atmos. Chem. Phys.*, 10, 4167–4186, doi:10.5194/acp-10-4167-2010, 2010. 13619

Huff Hartz, K. E., Rosenorn, T., Ferchak, S., Raymond, T., Bilde, M., Donahue, N., and Pandis, S.: Cloud condensation nuclei activation of monoterpene and sesquiterpene secondary organic aerosol, *J. Geophys. Res.*, 110, D14208, doi:10.1029/2004JD005754, 2005. 13620, 13632

Huffman, J. A., Docherty, K. S., Aiken, A. C., Cubison, M. J., Ulbrich, I. M., DeCarlo, P. F., Sueper, D., Jayne, J. T., Worsnop, D. R., Ziemann, P. J., and Jimenez, J. L.: Chemically-resolved aerosol volatility measurements from two megacity field studies, *Atmos. Chem. Phys.*, 9, 7161–7182, doi:10.5194/acp-9-7161-2009, 2009. 13624

Huffman, J. A., Ziemann, P., Jayne, J., Worsnop, D., and Jimenez, J.: Development and characterization of a fast-stepping/scanning thermodenuder for chemically-resolved aerosol volatility measurements, *Aerosol Sci. Technol.*, 42, 395–407, doi:10.1080/02786820802104981, 2008. 13624

Jimenez, J. L., Canagaratna, M. R., Donahue, N. M., Prevot, A. S. H., Zhang, Q., Kroll, J. H., Decarlo, P. F., Allan, J. D., Coe, H., Ng, N. L., Aiken, A. C., Docherty, K. S., Ulbrich, I. M., Grieshop, A. P., Robinson, A. L., Duplissy, J., Smith, J. D., Wilson, K. R., Lanz, V. A., Hueglin,

C., Sun, Y. L., Tian, J., Laaksonen, A., Raatikainen, T., Rautiainen, J., Vaattovaara, P., Ehn, M., Kulmala, M., Tomlinson, J. M., Collins, D. R., Cubison, M. J., Dunlea, J., Huffman, J. A., Onasch, T. B., Alfarra, M. R., Williams, P. I., Bower, K., Kondo, Y., Schneider, J., Drewnick, F., Borrmann, S., Weimer, S., Demerjian, K., Salcedo, D., Cottrell, L., Griffin, R., Takami, A., Miyoshi, T., Hatakeyama, S., Shimono, A., Sun, J. Y., Zhang, Y. M., Dzepina, K., Kimmel, J. R., Sueper, D., Jayne, J. T., Herndon, S. C., Trimborn, A. M., Williams, L. R., Wood, E. C., Middlebrook, A. M., Kolb, C. E., Baltensperger, U., and Worsnop, D. R.: Evolution of organic aerosols in the atmosphere, *Science*, 326, 1525–1529, doi:10.1126/science.1180353, 2009. 13619, 13620, 13624, 13628, 13632

Kanakidou, M., Seinfeld, J. H., Pandis, S. N., Barnes, I., Dentener, F. J., Facchini, M. C., Van Dingenen, R., Ervens, B., Nenes, A., Nielsen, C. J., Swietlicki, E., Putaud, J. P., Balkanski, Y., Fuzzi, S., Horth, J., Moortgat, G. K., Winterhalter, R., Myhre, C. E. L., Tsigaridis, K., Vignati, E., Stephanou, E. G., and Wilson, J.: Organic aerosol and global climate modelling: a review, *Atmos. Chem. Phys.*, 5, 1053–1123, doi:10.5194/acp-5-1053-2005, 2005. 13619

Kang, E., Root, M. J., Toohey, D. W., and Brune, W. H.: Introducing the concept of Potential Aerosol Mass (PAM), *Atmos. Chem. Phys.*, 7, 5727–5744, doi:10.5194/acp-7-5727-2007, 2007. 13620

King, S. M., Rosenoern, T., Shilling, J. E., Chen, Q., Wang, Z., Biskos, G., McKinney, K. A., Pöschl, U., and Martin, S. T.: Cloud droplet activation of mixed organic-sulfate particles produced by the photooxidation of isoprene, *Atmos. Chem. Phys.*, 10, 3953–3964, doi:10.5194/acp-10-3953-2010, 2010. 13633

King, S. M., Rosenoern, T., Shilling, J. E., Chen, Q., and Martin, S. T.: Cloud condensation nucleus activity of secondary organic aerosol particles mixed with sulfate, *Geophys. Res. Lett.*, 34, L24806, doi:10.1029/2007GL030390, 2007. 13632, 13633

Krevelen, D. V.: Graphical-statistical method for the study of structure and reaction processes of coal, *Fuel*, 24, 269–284, 1950. 13620

Kroll, J. and Seinfeld, J.: Chemistry of secondary organic aerosol: Formation and evolution of low-volatility organics in the atmosphere, *Atmos. Environ.*, 42, 3593–3624, 2008. 13619

Kroll, J. H., Smith, J. D., Che, D. L., Kessler, S. H., Worsnop, D. R., and Wilson, K. R.: Measurement of fragmentation and functionalization pathways in the heterogeneous oxidation of oxidized organic aerosol, *Phys. Chem. Chem. Phys.*, 11, 8005, doi:10.1039/b905289e, 2009. 13627

Kroll, J. H., Donahue, N. M., Jimenez, J. L., Kessler, S. H., Canagaratna, M. R., Wilson, K. R.,

Studies of chemical composition and CCN activity of SOA

A. T. Lambe et al.

Title Page

Abstract

Introduction

Conclusions

References

Tables

Figures

◀

▶

◀

▶

Back

Close

Full Screen / Esc

Printer-friendly Version

Interactive Discussion



Studies of chemical composition and CCN activity of SOA

A. T. Lambe et al.

Title Page

Abstract

Introduction

Conclusions

References

Tables

Figures

◀

▶

◀

▶

Back

Close

Full Screen / Esc

Printer-friendly Version

Interactive Discussion



Altieri, K. E., Mazzoleni, L. R., Wozniak, A. S., Bluhm, H., Mysak, E. R., Smith, J. D., Kolb, C. E., and Worsnop, D. R.: Carbon oxidation state as a metric for describing the chemistry of atmospheric organic aerosol, *Nature Chemistry*, 3, 133–139, doi:10.1038/nchem.948, 2011. 13619, 13625

5 Lambe, A. T., Ahern, A. T., Williams, L. R., Slowik, J. G., Wong, J. P. S., Abbatt, J. P. D., Brune, W. H., Ng, N. L., Wright, J. P., Croasdale, D. R., Worsnop, D. R., Davidovits, P., and Onasch, T. B.: Characterization of aerosol photooxidation flow reactors: heterogeneous oxidation, secondary organic aerosol formation and cloud condensation nuclei activity measurements, *Atmos. Meas. Tech.*, 4, 445–461, doi:10.5194/amt-4-445-2011, 2011. 13620, 13622

10 Lance, S., Medina, J., Smith, J., and Nenes, A.: Mapping the operation of the DMT continuous flow CCN counter, *Aerosol Sci. Technol.*, 40, 242–254, doi:10.1080/02786820500543290, 2006. 13624

Lanz, V. A., Alfarra, M. R., Baltensperger, U., Buchmann, B., Hueglin, C., and Prévôt, A. S. H.: Source apportionment of submicron organic aerosols at an urban site by factor analytical modelling of aerosol mass spectra, *Atmos. Chem. Phys.*, 7, 1503–1522, doi:10.5194/acp-7-1503-2007, 2007. 13619

Lee, A. K. Y., Herckes, P., Leaitch, W. R., Macdonald, A. M., and Abbatt, J. P. D.: Aqueous OH oxidation of ambient organic aerosol and cloud water organics: formation of highly oxidized products, *Geophys. Res. Lett.*, submitted, 2011. 13626, 13627

20 Liu, X. and Wang, J.: How important is organic aerosol hygroscopicity to aerosol indirect forcing?, *Environ. Res. Lett.*, 5, 044010, doi:10.1088/1748-9326/5/4/044010, 2010. 13620

Mao, J., Ren, X., Brune, W. H., Olson, J. R., Crawford, J. H., Fried, A., Huey, L. G., Cohen, R. C., Heikes, B., Singh, H. B., Blake, D. R., Sachse, G. W., Diskin, G. S., Hall, S. R., and Shetter, R. E.: Airborne measurement of OH reactivity during INTEX-B, *Atmos. Chem. Phys.*, 9, 163–173, doi:10.5194/acp-9-163-2009, 2009. 13622

25 Massoli, P., Lambe, A. T., Ahern, A. T., Williams, L. R., Ehn, M., Mikkilä, J., Canagaratna, M. R., Brune, W. H., Onasch, T. B., Jayne, J. T., Petäjä, T., Kulmala, M., Laaksonen, A., Kolb, C. E., Davidovits, P., and Worsnop, D. R.: Relationship between aerosol oxidation level and hygroscopic properties of laboratory generated secondary organic aerosol (SOA) particles, *Geophys. Res. Lett.*, 37, L24801, doi:10.1029/2010GL045258, 2010. 13620, 13630, 13631, 13632

30 Mazzoleni, L., Ehrmann, B., Shen, X., Marshall, A., and Jr, J. C.: Water-soluble atmospheric organic matter in fog: exact masses and chemical formula identification by ultrahigh-resolution

Studies of chemical composition and CCN activity of SOA

A. T. Lambe et al.

Title Page

Abstract

Introduction

Conclusions

References

Tables

Figures

◀

▶

◀

▶

Back

Close

Full Screen / Esc

Printer-friendly Version

Interactive Discussion



Fourier transform ion cyclotron resonance mass spectrometry, *Environ. Sci. Technol.*, **44**, 3690–3697, 2010. 13619

McKinley, J.: Permeation tubes: A simple path to very complex gas mixtures, *Gases & Instrumentation*, 22–26, www.gasesmag.com, 2008. 13623

5 Morgan, W. T., Allan, J. D., Bower, K. N., Highwood, E. J., Liu, D., McMeeking, G. R., Northway, M. J., Williams, P. I., Krejci, R., and Coe, H.: Airborne measurements of the spatial distribution of aerosol chemical composition across Europe and evolution of the organic fraction, *Atmos. Chem. Phys.*, **10**, 4065–4083, doi:10.5194/acp-10-4065-2010, 2010. 13628

10 Ng, N. L., Canagaratna, M. R., Zhang, Q., Jimenez, J. L., Tian, J., Ulbrich, I. M., Kroll, J. H., Docherty, K. S., Chhabra, P. S., Bahreini, R., Murphy, S. M., Seinfeld, J. H., Hildebrandt, L., Donahue, N. M., DeCarlo, P. F., Lanz, V. A., Prvt, A. S. H., Dinar, E., Rudich, Y., and Worsnop, D. R.: Organic aerosol components observed in Northern Hemispheric datasets from Aerosol Mass Spectrometry, *Atmos. Chem. Phys.*, **10**, 4625–4641, doi:10.5194/acp-10-4625-2010, 2010. 13619, 13625, 13626, 13627, 13632

15 Ng, N., Canagaratna, M., Jimenez, J., Zhang, Q., Ulbrich, I., and Worsnop, D.: Real-time methods for estimating organic component mass concentrations from aerosol mass spectrometer data, *Environ. Sci. Technol.*, **45**, 910–916, 2011a. 13628, 13650

20 Ng, N. L., Canagaratna, M. R., Jimenez, J. L., Chhabra, P. S., Seinfeld, J. H., and Worsnop, D. R.: Changes in organic aerosol composition with aging inferred from aerosol mass spectra, *Atmos. Chem. Phys. Discuss.*, **11**, 7095–7112, doi:10.5194/acpd-11-7095-2011, 2011b. 13620, 13628, 13629, 13630, 13651

Nishino, N., Arey, J., and Atkinson, R.: Yields of glyoxal and ring-cleavage co-products from the OH radical-initiated reactions of naphthalene and selected alkylnaphthalenes, *Environ. Sci. Technol.*, **43**, 8554–8560, 2009. 13625

25 Nishino, N., Arey, J., and Atkinson, R.: Formation yields of glyoxal and methylglyoxal from the gas-phase OH radical-initiated reactions of toluene, xylenes, and trimethylbenzenes as a function of NO₂ concentration, *J. Phys. Chem. A*, **114**, 10140–10147, 2010. 13625

Paatero, P. and Tapper, U.: Positive Matrix Factorization: A non-negative factor model with optimal utilization of error estimates of data values, *Environmetrics*, **5**, 111–126, 1994. 13627

30 Petters, M. D. and Kreidenweis, S. M.: A single parameter representation of hygroscopic growth and cloud condensation nucleus activity, *Atmos. Chem. Phys.*, **7**, 1961–1971, doi:10.5194/acp-7-1961-2007, 2007. 13624

Petters, M. D., Prenni, A. J., Kreidenweis, S. M., Demott, P. J., Matsunaga, A., Lim, Y. B., and

Studies of chemical composition and CCN activity of SOA

A. T. Lambe et al.

Title Page

Abstract

Introduction

Conclusions

References

Tables

Figures

◀

▶

◀

▶

Back

Close

Full Screen / Esc

Printer-friendly Version

Interactive Discussion



- Ziemann, P. J.: Chemical aging and the hydrophobic-to-hydrophilic conversion of carbonaceous aerosol, *Geophys. Res. Lett.*, 33, L24806, doi:10.1029/2006GL027249, 2006. 13620
- Petters, M. D., Kreidenweis, S. M., Prenni, A. J., Sullivan, R. C., Carrico, C. M., Koehler, K. A., and Ziemann, P. J.: Role of molecular size in cloud droplet activation, *Geophys. Res. Lett.*, 36, L22801, doi:10.1029/2009GL040131, 2009. 13631
- Poulain, L., Wu, Z., Petters, M. D., Wex, H., Hallbauer, E., Wehner, B., Massling, A., Kreidenweis, S. M., and Stratmann, F.: Towards closing the gap between hygroscopic growth and CCN activation for secondary organic aerosols – Part 3: Influence of the chemical composition on the hygroscopic properties and volatile fractions of aerosols, *Atmos. Chem. Phys.*, 10, 3775–3785, doi:10.5194/acp-10-3775-2010, 2010. 13620
- Prenni, A. J., Petters, M. D., Kreidenweis, S. M., Demott, P. J., and Ziemann, P. J.: Cloud droplet activation of secondary organic aerosol, *J. Geophys. Res.*, 112, D10223, doi:10.1029/2006JD007963, 2007. 13632, 13633
- Presto, A., Miracolo, M., Kroll, J., Worsnop, D., Robinson, A., and Donahue, N.: Intermediate-volatility organic compounds: a potential source of ambient oxidized organic aerosol, *Environ. Sci. Technol.*, 43, 4744–4749, 2009. 13620
- Prisle, N. L., Raatikainen, T., Laaksonen, A., and Bilde, M.: Surfactants in cloud droplet activation: mixed organic-inorganic particles, *Atmos. Chem. Phys.*, 10, 5663–5683, doi:10.5194/acp-10-5663-2010, 2010. 13633
- Roberts, G. C. and Nenes, A.: A continuous-flow streamwise thermal-gradient CCN chamber for atmospheric measurements, *Aerosol Sci. Technol.*, 39, 206–221, doi:10.1080/027868290913988, 2005. 13624
- Robinson, A. L., Donahue, N. M., Shrivastava, M. K., Weitkamp, E. A., Sage, A. M., Grieshop, A. P., Lane, T. E., Pierce, J. R., and Pandis, S. N.: Rethinking organic aerosols: semivolatile emissions and photochemical aging, *Science*, 315, 1259–1262, doi:10.1126/science.1133061, 2007. 13620
- Shilling, J., King, S., Mochida, M., Worsnop, D., and Martin, S.: Mass spectral evidence that small changes in composition caused by oxidative aging processes alter aerosol CCN properties, *J. Phys. Chem. A*, 111, 3358–3368, 2007. 13620
- Sorooshian, A., Varutbangkul, V., Brechtel, F. J., Ervens, B., Feingold, G., Bahreini, R., Murphy, S. M., Holloway, J. S., Atlas, E. L., Buzorius, G., Jonsson, H., Flagan, R. C., and Seinfeld, J. H.: Oxalic acid in clear and cloudy atmospheres: analysis of data from International Consortium for Atmospheric Research on Transport and Transformation 2004, *J. Geophys. Res.*,

Studies of chemical composition and CCN activity of SOA

A. T. Lambe et al.

Title Page

Abstract

Introduction

Conclusions

References

Tables

Figures

◀

▶

◀

▶

Back

Close

Full Screen / Esc

Printer-friendly Version

Interactive Discussion



111, D23S45, doi:10.1029/2005JD006880, 2006. 13625

Takegawa, N., Miyakawa, T., Kawamura, K., and Kondo, Y.: Contribution of selected dicarboxylic and ω -oxocarboxylic acids in ambient aerosol to the m/z 44 signal of an Aerodyne aerosol mass spectrometer, *Aerosol Sci. Technol.*, 41, 418–437, doi:10.1080/02786820701203215, 2007. 13625

Ulbrich, I., Lechner, M., and Jimenez, J.: AMS Spectral Database, <http://cires.colorado.edu/jimenez-group/AMSsd/>, last access: 2011. 13628

Ulbrich, I. M., Canagaratna, M. R., Zhang, Q., Worsnop, D. R., and Jimenez, J. L.: Interpretation of organic components from Positive Matrix Factorization of aerosol mass spectrometric data, *Atmos. Chem. Phys.*, 9, 2891–2918, doi:10.5194/acp-9-2891-2009, 2009. 13628

Varutbangkul, V., Brechtel, F. J., Bahreini, R., Ng, N. L., Keywood, M. D., Kroll, J. H., Flanagan, R. C., Seinfeld, J. H., Lee, A., and Goldstein, A. H.: Hygroscopicity of secondary organic aerosols formed by oxidation of cycloalkenes, monoterpenes, sesquiterpenes, and related compounds, *Atmos. Chem. Phys.*, 6, 2367–2388, doi:10.5194/acp-6-2367-2006, 2006. 13620

Volkamer, R., Platt, U., and Wirtz, K.: Primary and secondary glyoxal formation from aromatics: experimental evidence for the bicycloalkyl-radical pathway from benzene, toluene, and p-xylene, *J. Phys. Chem. A*, 105, 7865–7874, 2001. 13625

Wang, J., Cubison, M. J., Aiken, A. C., Jimenez, J. L., and Collins, D. R.: The importance of aerosol mixing state and size-resolved composition on CCN concentration and the variation of the importance with atmospheric aging of aerosols, *Atmos. Chem. Phys.*, 10, 7267–7283, doi:10.5194/acp-10-7267-2010, 2010. 13620

Wozniak, A. S., Bauer, J. E., Sleighter, R. L., Dickhut, R. M., and Hatcher, P. G.: Technical Note: Molecular characterization of aerosol-derived water soluble organic carbon using ultrahigh resolution electrospray ionization Fourier transform ion cyclotron resonance mass spectrometry, *Atmos. Chem. Phys.*, 8, 5099–5111, doi:10.5194/acp-8-5099-2008, 2008. 13619

Zhang, Q., Alfarra, M., Worsnop, D., Allan, J., Coe, H., Canagaratna, M., and Jimenez, J.: Deconvolution and quantification of hydrocarbon-like and oxygenated organic aerosols based on aerosol mass spectrometry, *Environ. Sci. Technol.*, 39, 4938–4952, 2005. 13619

Studies of chemical composition and CCN activity of SOA

A. T. Lambe et al.

Table 1. f_{44} and f_{43} for PAM-generated SOA/OPOA. Column 1 lists SOA/OPOA precursor, and “maxOH” and “minOH” denote measurements at the maximum ($\sim 2 \times 10^{12}$ molec cm $^{-3}$ s) and minimum ($\sim 1 \times 10^{11}$ molec cm $^{-3}$ s) OH exposures, respectively. Typical measurement uncertainty is 5–10%.

Precursor	$f_{44,\text{maxOH}}$	$f_{43,\text{maxOH}}$	$f_{44,\text{minOH}}$	$f_{43,\text{minOH}}$
<i>n</i> -C ₁₀	0.27	0.043	0.038	0.11
<i>n</i> -C ₁₇	0.30	0.030	0.025	0.10
diesel fuel	0.26	0.05	0.06	0.11
lubricating oil	0.035	0.087	0.0038	0.10
BES	0.055	0.076	0.013	0.054
isoprene	0.12	0.12	0.077	0.16
α -pinene	0.28	0.064	0.085	0.16
β -pinene	0.27	0.044	0.065	0.11
longifolene	0.21	0.045	0.040	0.055
glyoxal	0.39	0.001	0.029	0.002
toluene	0.31	0.021	0.16	0.09
<i>m</i> -xylene	0.30	0.048	0.095	0.17
mesitylene	0.25	0.079	0.069	0.21
naphthalene	0.29	0.010	0.073	0.0079

[Title Page](#)
[Abstract](#)
[Introduction](#)
[Conclusions](#)
[References](#)
[Tables](#)
[Figures](#)
[Back](#)
[Close](#)
[Full Screen / Esc](#)
[Printer-friendly Version](#)
[Interactive Discussion](#)


Studies of chemical composition and CCN activity of SOA

A. T. Lambe et al.

Title Page

Abstract

Introduction

Conclusions

References

Tables

Figures

I◀

▶I

◀

▶

Back

Close

Full Screen / Esc

Printer-friendly Version

Interactive Discussion



Table 2. Average Van Krevelen slopes $[(H/C)/(O/C)]$ of PAM-generated SOA/OPOA. Typical slope uncertainty is 10–20 %.

Precursor	Slope
<i>n</i> -C ₁₀	−0.80
<i>n</i> -C ₁₇	−0.60
diesel fuel	−0.64
lubricating oil	−1.7
BES	−0.87
isoprene	−0.87
α -pinene	−0.48
β -pinene	−0.57
longifolene	−0.45
glyoxal	−1.2
toluene	−0.48
m-xylene	−0.46
mesitylene	−0.55
naphthalene	−0.05

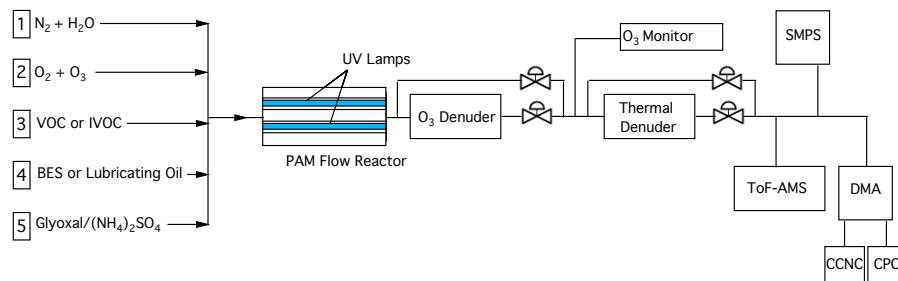


Fig. 1. Simplified schematic of experimental setup. As indicated, input lines 1 and 2 provide carrier gases (N_2 , O_2) and OH radical precursors (O_3 , H_2O). Line 3, 4, and 5 provide precursors for SOA and OPOA production as described in Sect. 2.3.

Studies of chemical composition and CCN activity of SOA

A. T. Lambe et al.

Title Page

Abstract Introduction

Conclusions References

Tables Figures

◀ ▶

◀ ▶

Back Close

Full Screen / Esc

Printer-friendly Version

Interactive Discussion



Studies of chemical composition and CCN activity of SOA

A. T. Lambe et al.

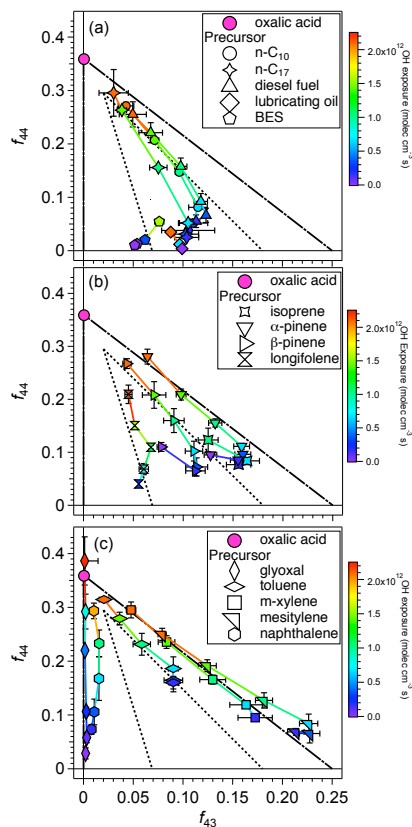


Fig. 2. f_{44} shown as a function of f_{43} for SOA and OPOA generated in the PAM from oxidation of (a) alkanes and BES, (b) biogenic terpenoids, and (c) aromatics and glyoxal. Symbols are colored by OH exposure; error bars represent $\pm 1\sigma$ in measurements. Measured f_{43} and f_{44} of oxalic acid shown for reference. Dashed lines indicate range of ambient f_{44} and f_{43} measurements, while dashed-and-dotted lines indicate range of laboratory PAM measurements. For details see text.

Title Page

Abstract

Introduction

Conclusions

References

Tables

Figures

◀

▶

◀

▶

Back

Close

Full Screen / Esc

Printer-friendly Version

Interactive Discussion



Studies of chemical composition and CCN activity of SOA

A. T. Lambe et al.

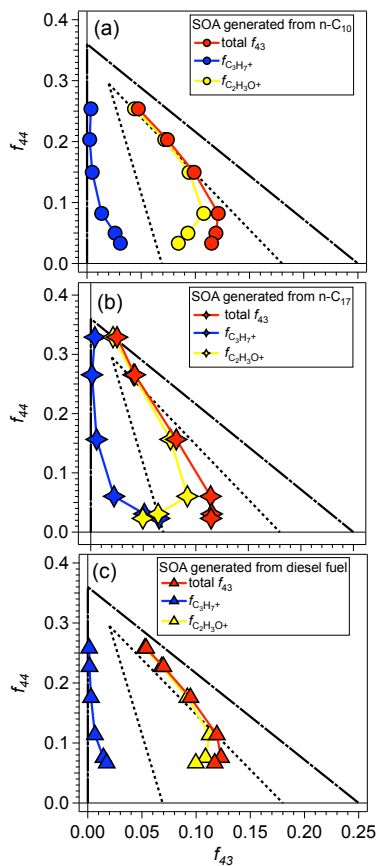


Fig. 3. f_{44} shown as a function of $f_{C_3H_7^+}$ (blue), $f_{C_2H_3O^+}$ (yellow), and total f_{43} (red) for SOA generated in the PAM from the oxidation of (a) n -C₁₀, (b) n -C₁₇, and (c) diesel fuel. Dashed lines indicate range of ambient f_{44} and f_{43} measurements, while dashed-and-dotted lines indicate range of laboratory PAM measurements.

Title Page

Abstract

Introduction

Conclusions

References

Tables

Figures

◀

▶

◀

▶

Back

Close

Full Screen / Esc

Printer-friendly Version

Interactive Discussion



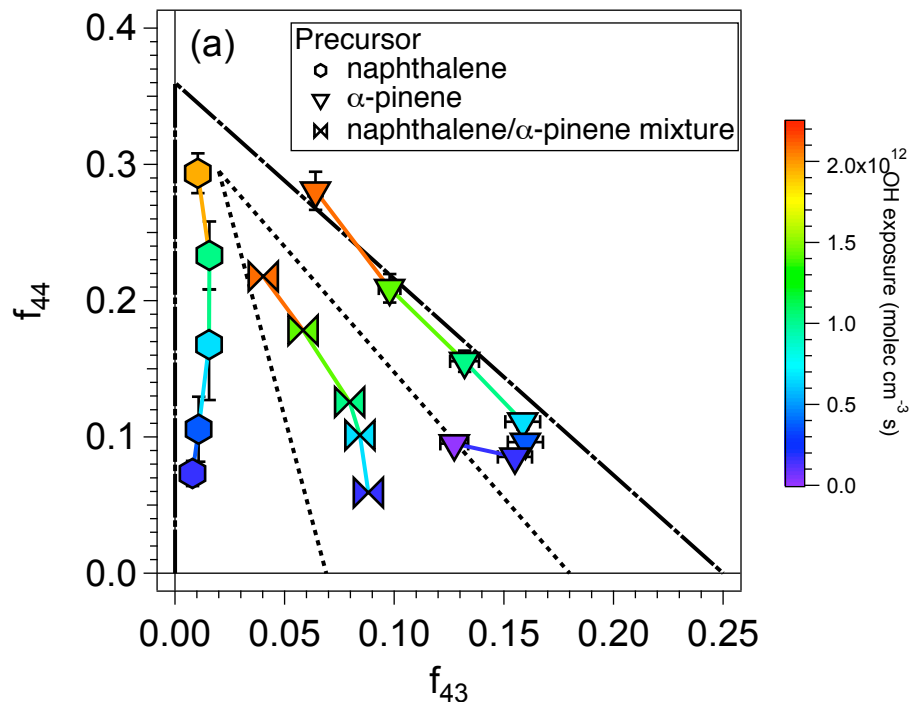


Fig. 4. f_{44} shown as a function of f_{43} for SOA generated in the PAM from a mixture of naphthalene and α -pinene. f_{43} and f_{44} data for SOA generated separately from naphthalene and α -pinene are replotted from Fig. 2. Error bars represent $\pm 1\sigma$ in measurements. Dashed lines indicate range of ambient f_{44} and f_{43} measurements, while dashed-and-dotted lines indicate range of laboratory PAM measurements.

Title Page

Abstract

Introduction

Conclusions

References

Tables

Figures

◀

▶

◀

▶

Back

Close

Full Screen / Esc

Printer-friendly Version

Interactive Discussion



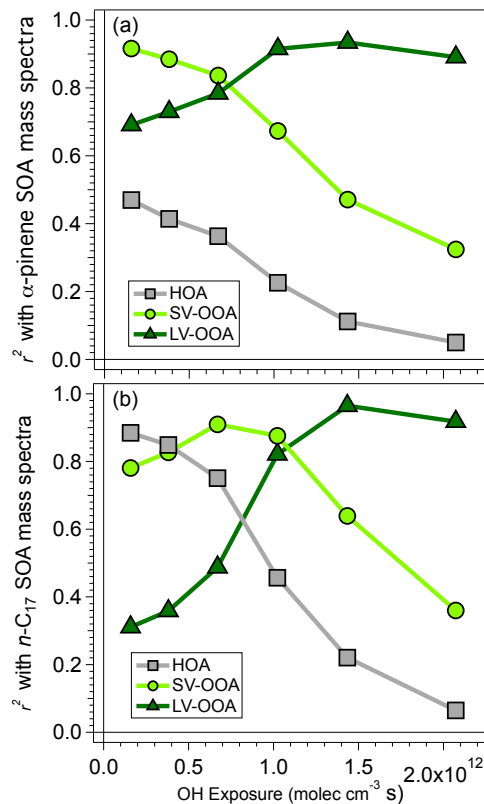


Fig. 5. Linear correlation coefficient (r^2) between mass spectra of PAM-generated (a) α -pinene SOA and (b) n -C₁₇ SOA and ambient hydrocarbon-like organic aerosol (HOA), ambient semivolatile OOA (SV-OOA), and ambient low-volatility OOA (LV-OOA) factors (Ng et al., 2011a) as a function of OH exposure in the PAM.

[Title Page](#)
[Abstract](#)
[Introduction](#)
[Conclusions](#)
[References](#)
[Tables](#)
[Figures](#)
[◀](#)
[▶](#)
[◀](#)
[▶](#)
[Back](#)
[Close](#)
[Full Screen / Esc](#)
[Printer-friendly Version](#)
[Interactive Discussion](#)


Studies of chemical composition and CCN activity of SOA

A. T. Lambe et al.

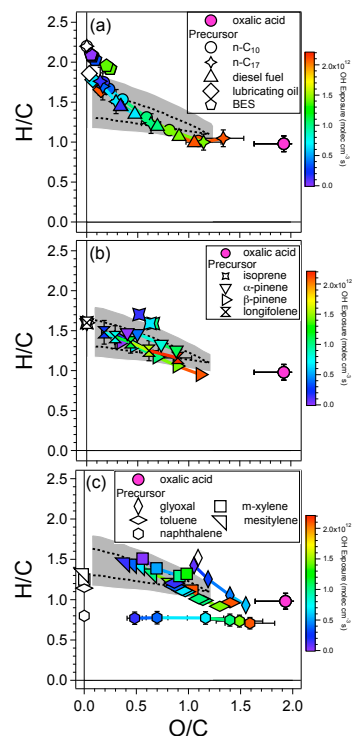


Fig. 6. Van Krevelen diagrams showing H/C ratio as a function of O/C ratio for SOA and OPOA generated in the PAM from **(a)** alkanes and BES, **(b)** biogenic terpenoids, and **(c)** aromatics and glyoxal. Symbols are colored by OH exposure, except for open symbols which represent unoxidized precursors. Measured H/C and O/C ratios of atomized oxalic acid are shown for reference. Representative error bars indicate $\pm 10\%$ uncertainty in H/C ratios and $\pm 15\%$ uncertainty in O/C ratios. Dashed lines represent range of H/C and O/C ratios in ambient OOA converted from corresponding f_{43} and f_{44} values; shaded grey region indicates conversion uncertainty as described in Ng et al. (2011b).

[Title Page](#)
[Abstract](#)
[Introduction](#)
[Conclusions](#)
[References](#)
[Tables](#)
[Figures](#)
[◀](#)
[▶](#)
[◀](#)
[▶](#)
[Back](#)
[Close](#)
[Full Screen / Esc](#)
[Printer-friendly Version](#)
[Interactive Discussion](#)


Studies of chemical composition and CCN activity of SOA

A. T. Lambe et al.

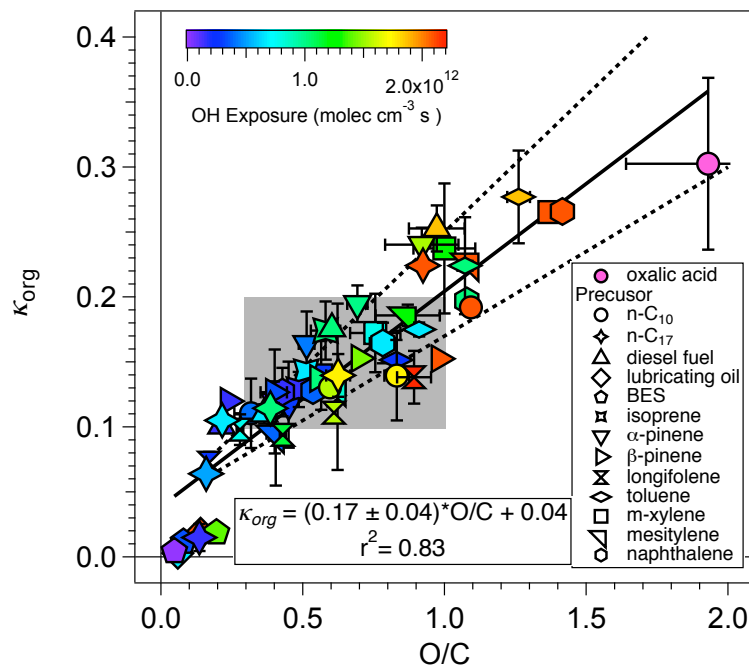


Fig. 7. CCN-derived hygroscopicity parameter (κ_{org}) shown as a function of O/C ratio for PAM-generated SOA and OPOA. Symbols are colored by OH exposure, and error bars represent $\pm 1\sigma$ in measurements. Measured κ_{org} of oxalic acid is shown for reference. Solid line indicates a linear fit to the data (slope = 0.17, intercept = 0.04, $r^2 = 0.83$) with $\pm 1\sigma$ confidence intervals.

Title Page

Abstract

Introduction

Conclusions

References

Tables

Figures

◀

▶

◀

▶

Back

Close

Full Screen / Esc

Printer-friendly Version

Interactive Discussion



Studies of chemical composition and CCN activity of SOA

A. T. Lambe et al.

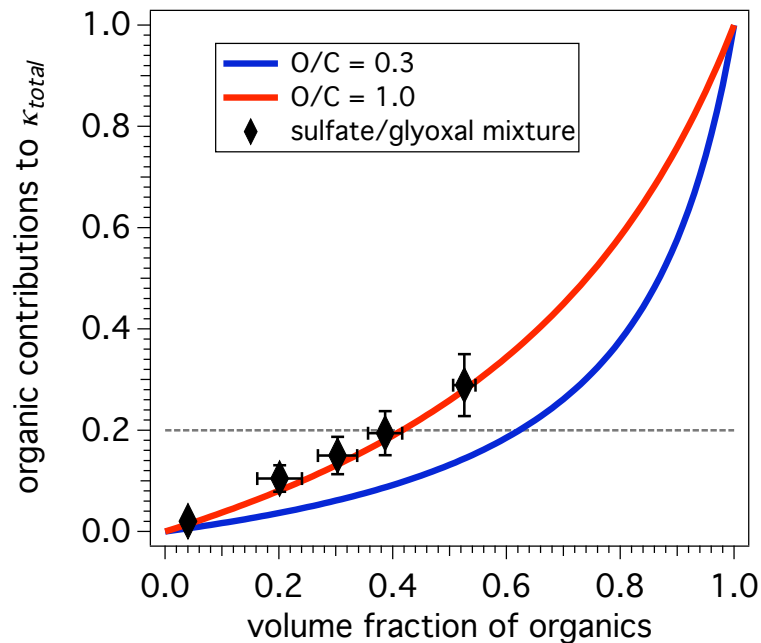


Fig. 8. Calculated contributions by OOA to κ_{total} in mixtures of ammonium sulfate and OOA shown as a function of organics volume fraction. Blue and red lines represent calculated κ -values for mixtures of ammonium sulfate and OOA with O/C ratios of 0.3 and 1.0, respectively. Black diamond symbols represent measured κ -values for a mixture of ammonium sulfate and glyoxal.

[Title Page](#)[Abstract](#)[Introduction](#)[Conclusions](#)[References](#)[Tables](#)[Figures](#)[◀](#)[▶](#)[◀](#)[▶](#)[Back](#)[Close](#)[Full Screen / Esc](#)[Printer-friendly Version](#)[Interactive Discussion](#)